Uncertainty assessment for the airborne nanoparticle collection efficiency of a TEM grid-equipped sampling system by Monte-Carlo calculation

Maiqi Xiang, Olivier Aguerre-Chariol, Martin Morgeneyer, Florian Philippe, Yan Liu, Christophe Bressot

Uncertainty assessment for the airborne nanoparticle collection efficiency of a TEM grid-equipped sampling system by Monte-Carlo calculation

Maiqi XIANG[1,2], Olivier AGUERRE-CHARIOL[2], Martin MORGENEYER[1], Florian PHILIPPE[1,2], Yan LIU[3], Christophe BRESSOT[2]

1. Génie de Procédés Industriels, Sorbonne Universités, Université de Technologie de Compiègne (UTC), Compiègne, France

2. Direction des Risques Chroniques, Institut National de l'Environnement Industriel et des Risques (INERIS), Verneuil en Halatte, France

3. Systèmes Temps-Réel et Informatique Embarquée, Sorbonne Universités, Université de Technologie de Compiègne (UTC), Compiègne, France

Abstract: A mini particle sampler (MPS) equipped with a transmission electron microscopy (TEM) grid enables convenient particle sampling to subsequent analysis. However, its sampling efficiency involves uncertainties, and accurate sampling efficiency is required for particle collection applications. In this study, the sampling efficiency uncertainties from measured data and models are quantified using Monte-Carlo methods. The Sobol variance-based sensitivity analysis is used to determine the contributions of parameters to the sampling efficiency uncertainties. The results reveal that the sampling efficiency uncertainties from experimental dispersion calibration and theoretical models are generally less than 1% and 9%, respectively. Most sampling efficiencies measured data are covered by the efficiency uncertainty range simulated by theoretical models. The pore size and flowrate contribute significantly to the sampling efficiency uncertainties, and require control to improve the precision of sampling efficiency. Besides, the Cunningham correction factor is also a sensitivity parameter. The utilization of proper models is crucial to support simulations for further process optimization. This study offers a quantitative method for nanoparticle collection efficiency analysis, which will help assess nanomaterials' workplace exposure.

Keywords: Monte-Carlo calculation; Sobol method; Transmission electron microscopy grid; Nanoparticle collection

1 Introduction

Using the TEM and related techniques to analyze airborne nanoparticles is a suitable approach for nanoparticle structure characterization [1, 2] and nano-exposure assessment [3-6]. Collecting particles directly onto TEM grids is an effective technique due to the direct microscopic analysis post-collection [7]. This approach to collect nanoparticles involves deposition mechanisms including electrostatic precipitation [8, 9], thermophoretic precipitation [10-12], and Brownian-diffusion [13, 14]. Recently, a low-cost, portable, and easy used instrument, TEM grid-equipped Mini Particle Sampler, was developed by Institute National de l'Environnement Industrial et des Risques (INERIS) and commercialized by the company Ecomesure, ~~,~~ as shown in Fig. 1 [15-17]. Researches on powder structure characterization [18-19] and nanomaterial exposure assessment [20-24] have validated the applicability of the MPS.

However, when collecting airborne nanoparticles by MPS, an accurate sampling efficiency is expected for subsequent quantitative analysis and application. The fluctuations among samples and the associated uncertainties in the experimental dispersion calibration require checks. Besides, the sampling efficiency of TEM grids can be modeled by filtration mechanisms [15]. The involved parameters bring uncertainties due to the measurement errors, insufficient observation data, imperfections in the manufacturing process [25]. For example, the parameter "pore size" brings uncertainties since the pores are not strictly uniformly distributed with the nominal diameter. Moreover, these models imply assumptions~~,~~ thereby accentuating uncertainty [25]. For example, the models assume different flow types and need to be carefully selected. Therefore, implementing uncertainty analysis in particle sampling is necessary.

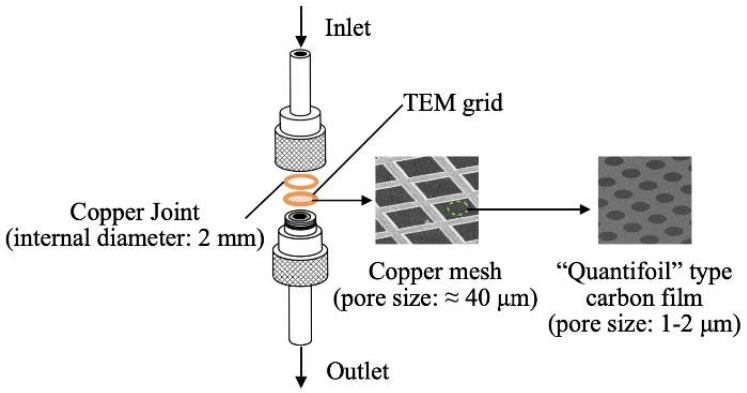

Fig. 1. Concept diagram of the TEM grid-equipped MPS

The Monte Carlo (MC) method is mostly used to compute the propagation of the random parameter uncertainties [26]. It is an advanced tool to facilitate the uncertainty analysis. Using the theory of probability, uncertain parameters can be described as variables for quantifying the sampling efficiency. Random samples of these parameters are generated according to their distributions. Each of these samples defines a deterministic problem, which is solved by generating an amount of data using a deterministic technique. Then, all these data are combined with statistics to access the output [27]. In addition, Sobol variance-based sensitivity analysis is used to indicate the contributions of the influence factors to the uncertainties. It is a global, variance-based method and can be used to explore how the output would be changed in response to variations in key parameters. This method is recommended by environmental regulations [28, 29]. Working within a probabilistic framework, it decomposes the variance of the model output into fractions attributed to individual parameters and the interactions between them.

In this study, the collection efficiency uncertainty of the TEM grid is evaluated using the MC method. Uncertainties from measured data and models are compared. The Sobol variance-based sensitivity analysis method is used to quantify the contributions of parameters to the sampling efficiency uncertainties. The here study proposes the first approach to perform quantitative analysis in nanoparticle collection.

2 Nanoparticle sampling efficiency of the TEM grid

2.1 Experimental sampling efficiency

The experimental design for checking the TEM grid-equipped MPS sampling efficiency is shown in Fig. 2. A membrane dryer generated clean, dry, and compressed air. Stable polydisperse salt solid particles, e.g., NaCl particles, were generated out of a 0.2 mmol/L NaCl solution using an atomizer (PALAS AGK 2000) by spray . 0.8 bar applied pressure was selected. Waterdrops were removed by two dryers, and the extra airflow was emitted through a HEPA filter. Quasi-monodisperse particles were selected

by an electrostatic classifier (3082, TSI) consists of an impactor, a neutralizer (3088), and a nano Differential Mobility Analyzer (DMA 3085A). The inertial impactor was used to remove large particles outside the instrument's measurement range. The neutralizer was utilized to establish an equilibrium charge state on the particles, with known percentages of particles carrying no charge, single charge, and multiple charges associated with positive and negative polarities entering the DMA [30, 31]. The DMA was used to remove the residuals of ultrapure water and choose particles within a narrow range of electrical mobility. Besides the mobility, particle diameters selected from the DMA also depend on the number of charges on the particles. That means singly charged particles with the chosen mobility diameter and bigger particles with multiply charges were selected. However, for particles smaller than 100 nm, the singly charged particles were much more than the multiply charged particles [32]. Thus most of the generated particles were monodisperse. Then the aerosolized particles were neutralized by another radioactive source (TSI 3087) upstream of the filter to avoid electrostatic effects on the filtration [33, 34]. Valves were utilized for inducing the flow to two symmetrically placed MPS, one with a TEM grid installed. Finally, the particle number concentration was measured by a Condensation Particle Counter (CPC 3787, TSI). The experimental sampling efficiency Exp corresponding to the selected size was calculated based on the particle number concentration [35]:

$$\mathrm{Exp} = 1 - C_{\mathrm{with}}/C_{\mathrm{without}} \quad (1)$$

Where C_{with} and C_{without} are the particle number concentration downstream of MPS, and measured by CPCwith and without TEM grid, respectively.

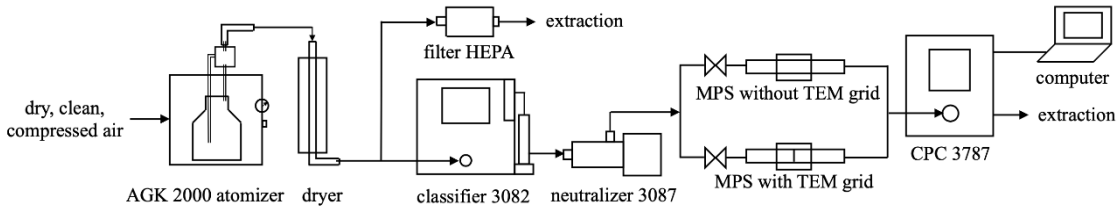

Fig. 2. Experimental set-up

According to the standard NF EN 13205-2, assessing the aerosol sampler performance [36]. Here the particle electrical mobility diameters were set as 5 nm, 7 nm, 10 nm, 20 nm, 30 nm, 40 nm, 60 nm, 80 nm, and 100 nm. Tests for each size were repeated three times. The sampling time of each step was 40 s.

2.2 Semi-empirical theoretical sampling efficiency

Theoretical models were used to simulate the filter collection efficiency by investigating the sampling mechanisms. According to Fig. 1, the TEM grid consists of a "Quantifoil" type holey carbon film and a copper mesh. Pores are almost uniform in size, hence the Nuclepore model was picked. According to Ogura et al. (2014) [17], the majority of the particles were captured by the carbon film because the pore size of the carbon film (1-2 μm) was much smaller than that of the copper mesh (≥ 40 μm). The collection efficiency of the copper mesh can be ignored. Assume that the carbon film thickness is L_{f}, the pore radius is r_0, and the pore area is A_0. The number of pores per surface unit of the carbon film is expressed as N_0: $N_0 = 1/(m+n)^2$. Where m is the pore size and n is the pore distance. The ratio of the opening of the pore to the total filter surface is the porosity P: $P = A_0 N_0 = \pi {r_0}^2 N_0$ [37, 38]. A cylindrical air stream with a radius r_{c} passes through a unitary pore, $r_{\mathrm{c}} = r_0/\sqrt{P}$ [37, 38]. Particles are collected onto the filter surface, or depositing on the wall of the filter pores. Distinct capture mechanisms were found: a) filter pore wall capture by Brownian diffusion, and b) interception; filter surface capture by c) Brownian diffusion, and d) impaction [39-41].

For the sampling system, high flowrates are unallowed (> 1 L/min) due to the load limit of the TEM grid and CPC. Hence low Reynold numbers are found in the airflow field. It is given by:

$$R_e = r_c U_0 / \upsilon \tag{2}$$

Where υ is the kinematic fluid viscosity. The face velocity U_0 is given by the flowrate Q and the section area of the filter:

$$U_0 = Q/(\pi/4){d_\mathrm{f}}^2 \tag{3}$$

d_f is the diameter of the TEM grid, and the nominal value is 2 mm.

Since the flow with a low Reynold number goes through thin circular pipe, the flow type can be considered ~~as~~ laminar flow. According to the flow conditions and TEM grids' structural characteristics, theoretical models for calculating collection efficiency have been chosen. Considering that flow slip at the filter pore wall could affect the filtration mechanism, especially might enhance the sampling efficiency in the intermediate crossover regime between Brownian diffusion and direct interception [42], the model of Marre [42] to calculate the pore wall deposition: combined efficiency of pore wall diffusion and interception E_DR was chosen [43].

$$E_\mathrm{DR} = \frac{4{y^*}^2}{1+4N_G}\left(1+2\frac{N_G}{y^*}\right) \tag{4}$$

Here,

$$N_G = N_g\left(1+N_g/2\right) \tag{5}$$

is a slip parameter N_g $(= l_g/r_0)$ based parameter, and lg is the slip length.

$$y^* = \frac{h^{2/3}+k^2\Gamma^2+(4N_R u_i - u_0)\Gamma h^{1/3}}{6\Gamma u_i h^{1/3}} \tag{6}$$

is the normalized distance with

$$h = \Gamma^2\left(54u_i^2 - k^3\Gamma + 6\sqrt{81u_i^2 - 3k^3\Gamma u_i}\right) \tag{7}$$

$$k = 2N_R u_i + u_0 \tag{8}$$

and

$$u_0 = \frac{2N_G}{1+4N_G} \tag{9}$$

$$u_i = \frac{1}{1+4N_G} \tag{10}$$

and

$$N_R = N_r(1 - N_r/2) \tag{11}$$

with N_r $(= r_\mathrm{P}/r_0)$ the normalized particle size, r_p is the particle radius.

Γ is a γ- based parameter calculated as:

$$\Gamma = \gamma\left(1 - 0.469\gamma^{-1/3} - 0.069\gamma^{-2/3}\right)^{-3/2} \tag{12}$$

For γ >100, and

$$\Gamma = 4\left[\begin{matrix}1 - 0.81904\exp(-3.6568\gamma^{-1}) - 0.09752\exp(-22.3045\gamma^{-1}) - 0.03248\exp(-56.95\gamma^{-1}) \\ -0.0157\exp(-107.6\gamma^{-1})\end{matrix}\right]^{-3/2} \tag{13}$$

For γ <100.γ determines the importance of axial convection with respect to radial diffusion:

$$\gamma = \frac{U_0 {r_0}^2}{DL_\mathrm{f}} \tag{14}$$

D is diffusion coefficient calculated by Stokes-Einstein equation [35,44]:

$$D = \frac{KTC_c}{6\pi\eta r_\mathrm{p}} \tag{15}$$

Where *K* is the Boltzmann constant; *T* is the temperature; η is the fluid dynamic viscosity. *Cc* is the Cunningham correction factor related to coefficients *a*, *b*, *c*, and K_n:

$$C_c = 1 + K_n[a + bexp(-c/K_n)] \tag{16}$$

K_n is Knudsen's number, a dimensionless number, defined as λ/r_P. λ is the fluid molecule mean free path.

For the diffusion efficiency due to particle deposition on the filter surface E_DS, the model of Manton [38] was selected:

$$E_\mathrm{DS} = 1 - exp\left\{-\frac{\alpha_1 \mathcal{D}^{2/3}}{[1+(\alpha_1/\alpha_2)\mathcal{D}^{7/15}]}\right\} \tag{17}$$

Where α_2 = 4.5, $\mathcal{D} = D/r_\mathrm{c}U_0$ is the normalized diffusion coefficient, α_1 is a parameter determined by the least-squares fitting, which related to the filter porosity:

$$\alpha_1 = 4.57 - 6.46P + 4.58P^2 \tag{18}$$

For impaction efficiency, the model of Pich [45] fits our sampling conditions. Laminar flow with parabolic streamlines and constant flow velocity in the flow direction are supposed in this model. It is calculated as:

$$E_{\mathrm{I}} = \frac{2\varepsilon_i}{1+\xi} - \left(\frac{\varepsilon_i}{1+\xi}\right)^2 \tag{19}$$

with

$$\varepsilon_i = 2Stk\sqrt{\xi} + 2Stk^2\xi exp\left[-\frac{1}{Stk\sqrt{\xi}}\right] - 2Stk^2\xi \tag{20}$$

$$\xi = \frac{\sqrt{P}}{1-\sqrt{P}} \tag{21}$$

Stk, the Stokes number is given by:

$$Stk = \frac{2C_c U_0 {r_{\mathrm{p}}}^2 \rho_{\mathrm{p}}}{9\eta r_0} \tag{22}$$

Where ρ_{p} is the particle density.

The overall collection efficiency is calculated from the different sampling mechanisms as [35]:

$$E_{\mathrm{th}} = 1 - (1 - E_{\mathrm{DR}})(1 - E_{\mathrm{DS}})(1 - E_{\mathrm{I}}) \tag{23}$$

3 Uncertainty analysis of TEM grid sampling efficiency

3.1 Uncertainty in the experimental dispersion calibration simulated by Monte Carlo

In the tests, the responses of CPC C_{down} and C_{up} are fluctuant in three scans. The experimental dispersion due to fluctuations among samples requires calibration. The calibrated data can be modeled as samples drawn from a Multivariate normal vector whose parameters are inferred from the raw measured particle counts [46]. The uncertainty is described using the MC method with a 95% confidence region over the nine diameters. 30000 samples are selected.

Let $\underset{C}{\rightarrow}$ be the 9×3 matrix of raw count samples containing 9-dimensional vectors (9 diameters) with 3 repeats:

$$\underset{C}{\rightarrow} = \begin{bmatrix} r1dp[1] & r2dp[1] & r3dp[1] \\ r1dp[2] & r2dp[2] & r3dp[2] \\ \vdots & \vdots & \vdots \\ r1dp[9] & r2dp[9] & r3dp[9] \end{bmatrix} \tag{24}$$

Let $R_{\vec{C}}$ be a 9×9 empirical correlation matrix containing the pairwise Pearson's linear correlation coefficient between each pair of columns in the matrix $\vec{C}^T$. It can be decomposed by singular value decomposition: $R_{\vec{C}} = U_{R_{\vec{C}}} \Sigma_{R_{\vec{C}}} U_{R_{\vec{C}}}^T$. $U_{R_{\vec{C}}}$ is the orthogonal matrix or rotation matrix of the singular value decomposition of $R_{\vec{C}}$. $\Sigma_{R_{\vec{C}}}$ is the diagonal matrix with non-negative real numbers known as the singular values of $R_{\vec{C}}$ on the diagonal. The measured samples $\tilde{\vec{C}}$ are modeled as:

$$\tilde{\vec{C}} = \mu_{\vec{C}} + \left(U_{R_{\vec{C}}} \sum_{R_{\vec{C}}}^{\frac{1}{2}} \mathcal{Z} \right) \circ \sigma_{\vec{C}} \tag{25}$$

$\mathcal{Z}$ is the Multivariate standard Gaussian distribution with $\mathcal{Z} \sim \mathcal{N}(0, \underset{I_9}{\Rightarrow})$. $\underset{I_9}{\Rightarrow}$ is a 9-dimensional unit matrix, and $\circ$ is the Hadamard product. $\mu_{\vec{C}}$ and $\sigma_{\vec{C}}$ are the 9-dimensional mean vector and standard deviation vector of $\vec{C}$, which are computed by:

$$\mu_{\vec{C}}[i] = \frac{1}{3} \sum_{r=1}^{3} \vec{C}[r,i], \qquad \sigma_{\vec{C}}[i] = \sqrt{\frac{1}{2} \sum_{r=1}^{3} \left(\vec{C}[r,i] - \mu_{\vec{C}}[i] \right)^2}, \qquad i = 1, \ldots, 9 \tag{26}$$

3.2 Model uncertainty simulated by Monte Carlo

Sampling efficiencies calculated by the theoretical models depend on parameters referring to filter properties, particle properties, flow conditions, and coefficients. All of these parameters are the sources of uncertainties. The combined uncertainties are propagated by the probability distribution of each parameter using the MC method with a 95% confidence region. 30000 samples are selected. Take the case of collecting NaCl nanoparticles by 1.2/1.3 "Quantifoil" holey carbon film 400 mesh copper TEM grid (1.2 μm nominal pore size with 1.3 μm nominal pore distance) at a flowrate of 0.6 L/min. The sources of uncertainties and the associated statistical models are listed in Table 1.

Table 1 List of the uncertainty sources and the associated modelings

Sources	Uncertainty model
K	Gaussian distribution with mean 1.380649 * 10^{-23} J/K

T	Arcsine distribution with mean 300 K
η	Gaussian distribution with mean 1.85 * 10^{-5} kg/(m·s)
l_g	Uniform distribution with mean 1.126 * 69.3 nm
L_f	Uniform distribution with mean 0.02 μm
r_0	Uniform distribution with mean 0.65 μm
N_0	Uniform distribution with mean 0.1276
ρ_P	Uniform distribution with mean 2111.15 kg/m^3
U_0	Uniform distribution with mean 2.9178 m/s
Cc	Multivariate Gaussian distribution with parameters identified from the literature

(1) Boltzmann constant K

The Boltzmann constant is used to calculate the diffusion coefficient. It is modeled as a Gaussian random variable with a mean of 1.380649×10^{-23} J/K. The relative standard uncertainties based on different independent measurements are less than 7.9×10^{-30} J/K, according to the 26th meeting of the General Conference on Weights and Measures (CGPM).

(2) Temperature T

Temperature is used to calculate the diffusion coefficient. 300 k was set in DMA. The temperature of aerosol passing through the TEM gird is modeled by an arcsine distribution (26.35+273.15 K, 27.35+273.15 K) [46, 47].

(3) Fluid dynamic viscosity η

Dynamic gas viscosity is used to calculate the diffusion coefficient and the Stokes number. It is expressed by the Sutherland formula

$$\eta = \eta_0 * \left(\frac{T}{T_0}\right)^{3/2} * \left(\frac{T_0 + B}{T + B}\right) \quad (27)$$

Where T_0 is 296.15 K, B is 110.4 K, the viscosity of air η_0 is modeled as a normal random variable $\eta_0 \sim N(\eta_0,$

$\sigma_{\eta_0}^2$) with a mean of 1.83245 $*$ 10^{-5} kg/(m·s) and standard deviation of 0.00069 $*$ 10^{-5} kg/(m·s) according to Birge [48].

(4) Slip length L_g

L_g is equal to $S\lambda$. S is a coefficient ranging from 1-1.4 [49], and 1.126 is recommended in recent years [50]. It is modeled by a uniform distribution, $S \sim$ U (1, 1.252). λ is described as:

$$\lambda = \lambda_0 \left(\frac{T}{T_0}\right)\left(\frac{P_0}{P_r}\right)\left(\frac{1 + B/T_0}{1 + B/T}\right) \tag{28}$$

Where λ_0 is 67.3 nm, P_0 is 101.3 kPa [51]. The pressure P_r set in DMA was 100 kPa. The pressure of aerosol passing through the TEM gird is modeled by an arcsine distribution (100-0.1 kPa, 100+0.1 kPa) [46].

(5) Filter thickness L_f

The nominal filter thickness provided by the manufacturer is 0.02 μm, it is modeled by a uniform distribution, $L_f \sim$ U (0.02-0.0005 μm, 0.02+0.0005 μm).

(6) Pore radius r_0

The pore radius of the 1.2/1.3 type grid provided by the manufacturer is 0.6 μm. The average value of at least 100 measurements is 0.65 μm. It is modeled by a uniform distribution, $r_0 \sim$ U (0.6 μm, 0.7 μm).

(7) Number of pores per surface unit of filter N_0

The pore size m and the pore distance n for calculating N_0 can be modeled by uniform distributions: $m \sim$ U (1.2 μm, 1.4 μm), $n \sim$ U (1.4 μm, 1.6 μm).

(8) Particle density ρ_p

The NaCl particle density is 2165 kg/m^3, and the purity provided by the manufacturer is 99.5%. Besides, the NaCl particle entering the DMA may be covered by waterdrops, which decreases its density. Hence, the NaCl particle density is modeled as a uniform distribution: $\rho_p \sim$ U (2046.466 kg/m^3, 2175.825 kg/m^3).

(9) Face velocity U_0

0.6 L/min flow goes through the filter by the control of the pump of CPC. The flowrate measured by the flowmeter inside of DMA is ranging between 0.5-0.6 L/min. Hence, the flowrate in the MPS is between 0.5-0.6 L/min. The corresponding face velocity can be modeled by a uniform distribution, $U_0 \sim$ U (2.6526 m/s, 3.1831 m/s).

(10) Cunningham correction factor *Cc*

Cc can be modeled by a multivariate Gaussian distribution with coefficients *a*, *b*, *c* identified from the literature. Table 2 summarizes some recently published values of these coefficients recommended by standard ISO 15900 [52].

Table 2 Recently published value of coefficients *a*, *b*, *c* for calculating Cunningham correction factor [52]

	a	b	C
Allen et Raabe (1985) [53]	1.142	0.558	0.999
Hutchins et al. (1995) [54]	1.231	0.4695	1.1783
Kim et al. (2005) [51]	1.165	0.483	0.997
Jung et al. (2012) [55]	1.165	0.48	1.001

Using simulations of L. Coquellin [46], the coefficients are modeled as truncated Gaussian distributions A, B, C, respectively. Let $\theta_{A,B,C} = \begin{pmatrix} A \\ B \\ C \end{pmatrix}$, $\theta^{A}_{A,B,C} = \begin{pmatrix} a_A \\ b_A \\ c_A \end{pmatrix}$, $\theta^{H}_{A,B,C} = \begin{pmatrix} a_H \\ b_H \\ c_H \end{pmatrix}$, $\theta^{J}_{A,B,C} = \begin{pmatrix} a_J \\ b_J \\ c_J \end{pmatrix}$, $\theta^{K}_{A,B,C} = \begin{pmatrix} a_K \\ b_K \\ c_K \end{pmatrix}$. A, H, J, K refer to the results of the four authors listed in Table 2.

$$\theta_{A,B,C} \sim \mathcal{N}\left[\theta^{low}_{A,B,C}, \theta^{up}_{A,B,C}\right]\left(\theta^{mean}_{A,B,C}, \sum \theta_{A,B,C}\right) \tag{29}$$

$$\theta^{low}_{A,B,C} = \begin{pmatrix} a_H \\ b_H \\ c_K \end{pmatrix} = \begin{pmatrix} 1.142 \\ 0.4695 \\ 0.997 \end{pmatrix}, \theta^{mean}_{A,B,C} = \begin{pmatrix} a_J \\ b_J \\ c_J \end{pmatrix} = \begin{pmatrix} 1.165 \\ 0.480 \\ 1.001 \end{pmatrix}, \theta^{up}_{A,B,C} = \begin{pmatrix} a_J \\ b_J \\ c_J \end{pmatrix} = \begin{pmatrix} 1.231 \\ 0.558 \\ 1.1783 \end{pmatrix} \tag{30}$$

The covariance matrix $\sum \theta_{A,B,C}$ is defined as:

$$\sum \theta_{A,B,C} = diag\left(\max\left(\left|\theta^{mean}_{A,B,C} - \theta^{low}_{A,B,C}\right|^2, \left|\theta^{up}_{A,B,C} - \theta^{mean}_{A,B,C}\right|^2\right)\right) \tag{31}$$

3.3 Model parameter sensitivity analysis using Sobol method

Modeling the sampling efficiency based on the above ten parameters: *Y = f (X)*. *X* is the vector of uncertain model

inputs (X_1, X_2, ... X_i, ... X_j, ... X_{10}), and Y is the output sampling efficiency. The input distributions are derived from the uncertainty models. The following functional decomposition scheme is considered [56]:

$$f = f_0 + \sum_i f_i + \sum_i \sum_{j>i} f_{ij} + \cdots + f_{12\ldots10} \tag{32}$$

The functions can be obtained from the conditional expectations:

$$f_0 = E(Y) \tag{33}$$

$$f_i = E_{\mathrm{X}_{\sim i}}(Y|X_i) - E(Y) \tag{34}$$

$$f_{ij} = E_{X_{\sim ij}}\left(Y\middle|X_i, X_j\right) - f_i - f_j - E(Y) \tag{35}$$

And similarly for higher orders.

The decomposition of total output variance to individual model parameters and their interactions can be written as:

$$V(Y) = \sum_{i=1}^{10} V_i + \sum_{i<j}^{10} V_{ij} + \cdots + V_{12\ldots10} \tag{36}$$

$$V_i = V_{X_i}\left(E_{\mathrm{X}_{\sim i}}(Y|X_i)\right) \tag{37}$$

$$V_{ij} = V_{X_{ij}}\left(E_{\mathrm{X}_{\sim ij}}\left(Y\middle|X_i, X_j\right)\right) - V_i - V_j \tag{38}$$

Where V_i is the first-order variance contribution of the i-th parameter, V_{ij} is the second-order contribution of the interaction between parameters i and j; and $V_{12\ldots10}$ contains all interactions higher than third-order, up to 10 total parameters.

Indicate the $X_{\sim i}$ notation as the set of all variables except X_i, the first-order index (S_i) and total-order index (S_{Ti}) [57] are defined as:

$$S_i = V_i/V(Y) \tag{39}$$

$$S_{T_i} = \frac{E_{X_{\sim i}}\left(V_{X_i}(Y|\mathrm{X}_{\sim i})\right)}{V(Y)} \tag{40}$$

The first-order index is the fraction of the total output variance caused by the parameter i. The total-order index measures the total contribution to the output variance of X_i, including its individual effects plus an estimate of its interactions with all other parameters.

A global sample of the parameter space is taken using a quasi-random Sobol sequence of values to achieve uniform coverage of the space [58, 59]. Two independent sampling matrices A and B, with N×10 dimensions, are assumed. The index i running from one to ten is the number of parameters, while the index j running from one to N is the number of simulations. Introducing matrix A_{B}^{i} where all columns are from A except the i-th column which is from B, Sobol sensitivity indices are calculated using the MC estimators as [60]:

$$V_{X_i}\left(E_{\mathrm{X}_{\sim i}}(Y|X_i)\right) \approx \frac{1}{N}\sum_{j=1}^{N} f(\mathrm{B})_j\left(f\left(\mathrm{A}_{\mathrm{B}}^{i}\right)_j - f(\mathrm{A})_j\right) \tag{41}$$

$$E_{\mathrm{X}_{\sim i}}\left(V_{X_i}(Y|\mathrm{X}_{\sim i})\right) \approx \frac{1}{2N}\sum_{j=1}^{N}\left(f(\mathrm{A})_j - f\left(\mathrm{A}_{\mathrm{B}}^{i}\right)_j\right)^2 \tag{42}$$

Parameters with sensitivity indices greater than 0.1 are considered significant. 1,000,000 samples were selected for convergence of the results.

4 Results and discussion

4.1 Uncertainty analysis of sampling efficiency

Fig. 3 shows the NaCl nanoparticle sampling efficiency uncertainties from experimental dispersion calibration and models. The uncertainties from experimental dispersion calibration (Exp) are simulated for 9 sizes and described according to the measured samples $\overrightarrow{\tilde{C}}$. The mean values are marked. The model uncertainties are described by an envelope of reliability (grey shadow) according to the parameter range. The figure also shows the mean overall efficiency (E_{th}) and the mean efficiency due to individual sampling mechanisms: E_{DS}, E_{DR}, and E_{I}. Table 3 shows the mean and uncertainty of experimental and theoretical sampling efficiency at different particle sizes. Here the uncertainty is calculated by 1/2 of the reliability envelope. Fig. 4 presents representative TEM images of 100 nm NaCl particles collected on the 1.2/1.3 carbon film TEM grid at the flowrate of 0.6 L/min. Analyzing with ImageJ,

most of the particles are homogeneously distributed with a size of 100 nm. Bigger particles observed may be caused by multiply charged.

Fig. 3.NaCl nanoparticle sampling efficiency uncertainties from experimental dispersion calibration and models

Table 3 Mean and uncertainty of sampling efficiency from measured data and theoretical models for monodisperse

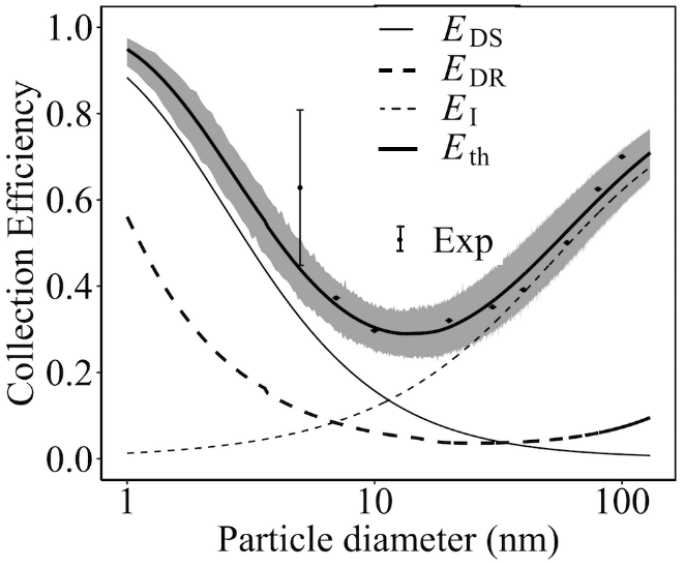

NaCl nanoparticles

Diameter		5 nm	7 nm	10 nm	20 nm	30 nm	40 nm	60 nm	80 nm	100 nm
Measurement	Mean	0.6282	0.3726	0.2972	0.3203	0.3516	0.3916	0.5008	0.6249	0.7000
	Uncertainty	0.18000	0.00012	0.00032	0.00009	0.00006	0.00001	0.00002	0.00006	0.00003
Model	Mean	0.4395	0.3568	0.3042	0.3045	0.3649	0.4263	0.5270	0.5997	0.6529
	Uncertainty	0.07035	0.06032	0.05101	0.06216	0.07282	0.08577	0.07509	0.06822	0.06731

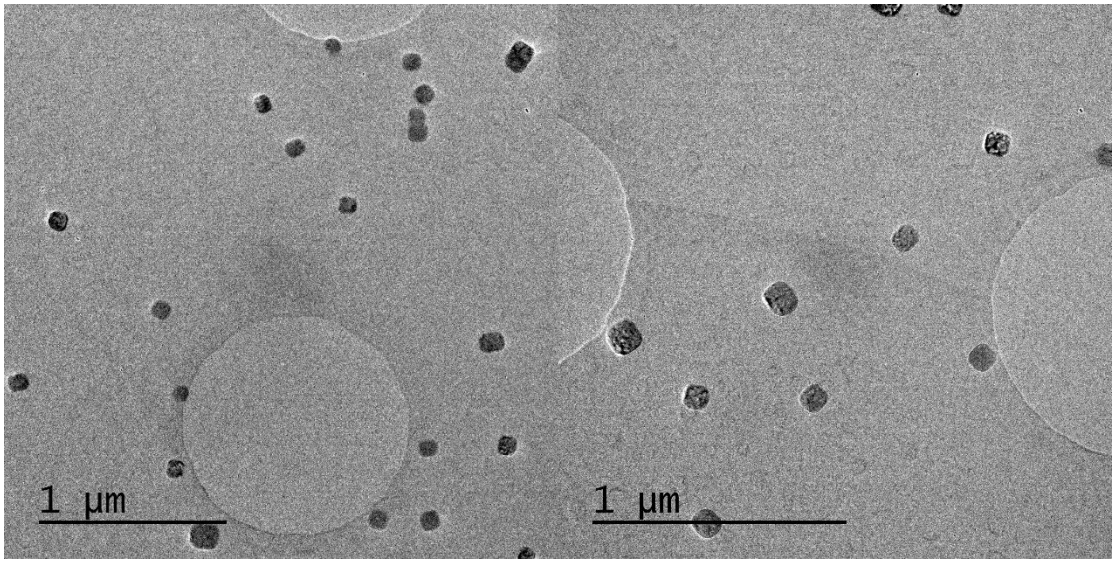

Fig. 4. Representative TEM images of NaCl particles with a mobility diameter of 100 nm

The sampling efficiency curve shows U-shape with a minimum. The uncertainties from measured data are mostly covered by those from the theoretical models. The averages of the experimental collection efficiencies are between 29% and 70%, with a minimum at 10 nm. The uncertainties from experimental dispersion calibration are mostly less than 1%. For 5 nm particles, a large error bar is found. The number concentration of 5 nm particles generated by the atomizer is too low to be constant, which increases the uncertainty. Besides, 5 nm is the detection limit of the used CPC [61]. The minimum of the efficiency calculated by the theoretical models (E_{th}) is about29% at a particle diameter of around 14 nm. This is consistent with the experimental results. The uncertainties of theoretical efficiencies for the nano-scale particles are between 5% and 9%. For particles smaller than 10 nm, the surface diffusion mechanism E_{DS} is significant for particle collection. And for those larger than 10 nm, impaction E_I is an essential mechanism. Collection efficiencies due to wall deposition E_{DR} are smaller than 12% for particles with diameters of 5-100 nm because of the small pore length and pore size ratio [62].

4.2 Sensitivity analysis of uncertain parameters

Fig. 5 shows the parameter sensitivity analysis of 10, 20, 50, and 100 nm NaCl particle theoretical collection efficiency.

The results depict that the primary source of uncertainties is pore size r_0 for particles in the nano-scale, with indices larger than 0.1. Pore size changes the collection efficiency due to diffusion and impaction. The uncertainties vary with particle sizes. *Cc* is significant for small particles, while for large particles, flowrate U_0 becomes an important parameter. *Cc* is used to correct Stokes's law because the no-slip boundary condition is violated for small particles moving with respect to the gaseous medium [53]. Different coefficients of *Cc* derived from the measurements bring great uncertainties to the model efficiency. The impaction mechanism, which is mainly affected by flowrate, significantly contributes to large particle collection.

Conversely, low indices are shown for the parameters: lg, L_f, ρ, η, T, K. Boltzmann constant K, slip length L_g, and fluid dynamic viscosity η are quasi-constants, bringing minor contributions to the sampling efficiency uncertainties. TEM grid thickness L_f and aerosol temperature T are also insensitive parameters due to their small ranges (0.02-0.0005 μm, 0.02+0.0005 μm; 26.35+273.15 K, 27.35+273.15 K). High purity decides a small particle density range, which leads to a minor uncertainty as well. For most of the parameters, the difference between the first-order index and total order index is large, which validates that these parameters affect sampling efficiency mainly by interacting with other parameters. The slightly negative first-order index estimation occurs when the index insignificantly differs from 0 63].

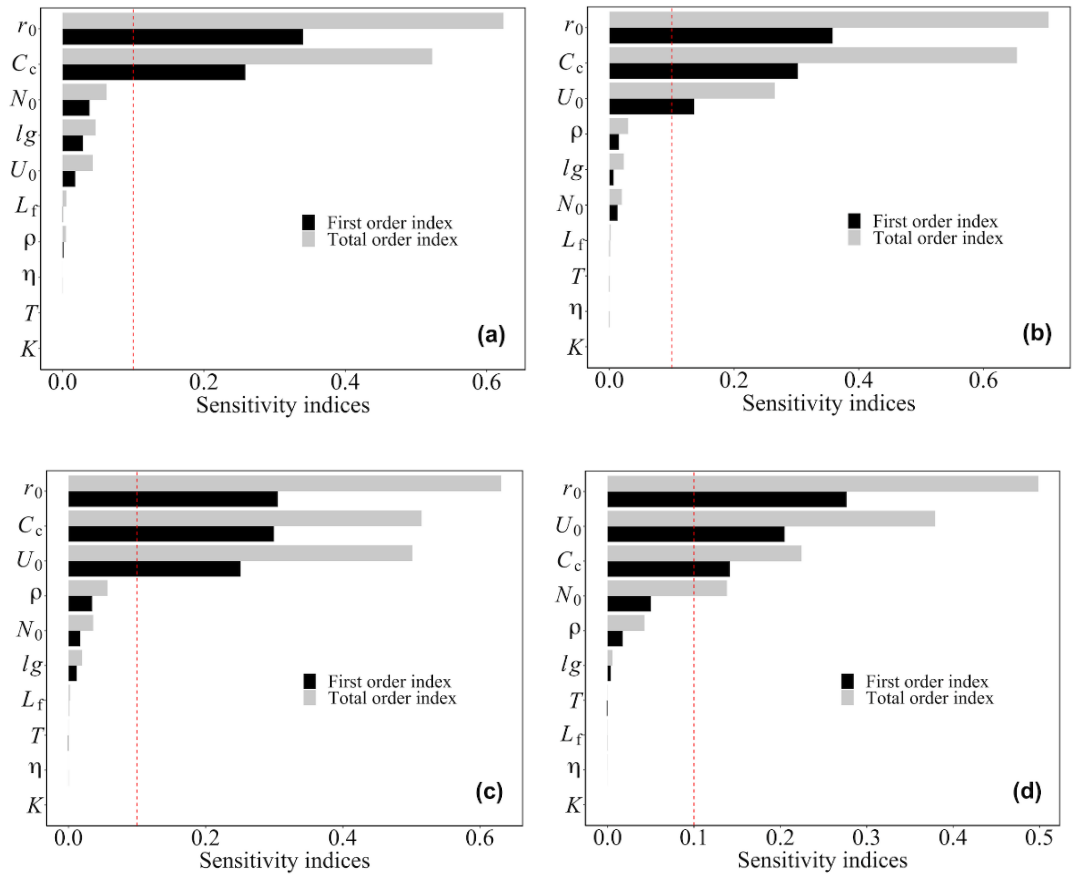

Fig. 5. Parameter sensitivity analysis of the NaCl particle sampling efficiency for sizes of (a) 10 nm; (b) 20 nm; (c) 50 nm; and (d) 100 nm.

4.3 The effects of sampling conditions

According to the sensitivity analysis results, pore size and flowrate are controllable sensitive parameters for sampling efficiency. Measurements have been carried out using different

TEM grids and flowrates. CsCl nanoparticles were generated by the atomizer filled with CsCl solution to explore the impact of particle density. The parameter ranges are shown in Table 4.

Table 4 Parameter ranges at different sampling conditions

Particle	Density range,	Grid	Pore size	Pore pitch	Flowrate set	Flowrate	Face velocity

type	kg/m^3	type	range, µm	range, µm	value, L/min	range, L/min	range, m/s
NaCl	2046.466-2175.825	2/2	1.8-2.2	1.9-2.0	0.6	0.6-0.75	2.9177-3.9788
NaCl	2046.466-2175.825	1.2/1.3	1.1-1.3	1.4-1.6	0.4	0.35-0.55	1.9629-2.3873
CsCl*	3769.657-4007.940	1.2/1.3	1.2-1.4	1.4-1.6	0.6	0.5-0.6	2.9177-3.9788

* Purity is 99.5%

Fig. 6 shows the collection efficiency uncertainties from measured data and theoretical models of the sampling system with a different pore size (5(a)), flowrate (5(b)), and collecting particles with a different density (5(c)). The results depict that

the uncertainties from the experimental dispersion calibration are smaller (mostly less than 1%) than those from the models for all these sampling conditions. For CsCl particle collection, the uncertainties from the measured data are mostly covered by the range from the models (6%-10%). The minimum efficiency increases with the particle density. Denser particles enhance the impaction efficiency by changing the value of *Stk*. For sampling conditions of the 2/2 type grid and 0.4 L/min flowrate, the measured data uncertainties are covered by the model uncertainties for small particles. Here *Cc* for calculating the "*Stk*" in the impaction efficiency model is 1, which decreases the model uncertainties (1%-9%). The choice of models and parameter values is essential for simulating the sampling efficiency. The minimum efficiency (mean) decreases (30% to 8%) with the increased pore size (0.6 to 1 µm) by reducing the diffusion and impaction efficiency. The minimum collection efficiency increases, and the corresponding size decreases as the flowrate increases. Increasing flowrate causes a greater probability of large particle impaction deposition, and small particles are less likely to be captured by diffusion [64].

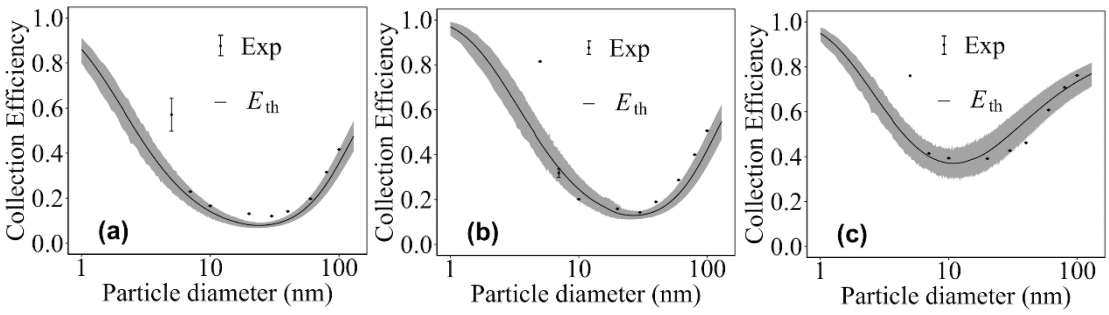

Fig. 6. Uncertainty analysis of 100 nm particle sampling efficiency in the conditions of (a) changing pore size; (b) changing flowrate; (c) changing particle density.

Fig. 7 shows the parameter sensitivity analysis of the theoretical collection efficiency for collecting 100 nm particles with a different pore size filter (6(a)), flowrate (6(b)), and density (6(c)). Pore size and flowrate are significant parameters with indices larger than 0.1. In addition, N_0 significantly contributes to the uncertainty for collecting the CsCl particles. The control of filter properties is of immediate importance for sampling efficiency quantification.

Fig. 7. Parameter sensitivity analysis of 100 nm particle sampling efficiency in the conditions of (a) changing pore size; (b) changing flowrate; (c) changing particle density.

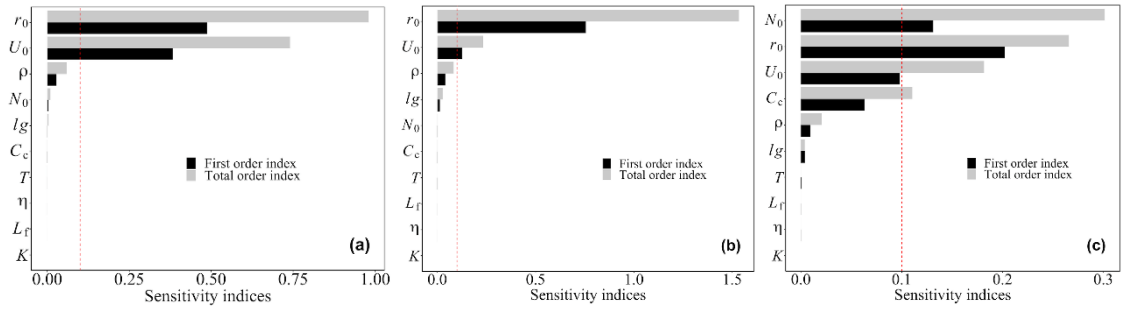

5 Conclusion

In this study, the TEM grid-equipped MPS sampling efficiencies were tested and modeled at different sampling conditions. The experimental dispersion due to fluctuations among different CPC scans was calibrated. Uncertainties from the calibrated data and models were simulated using the Monte-Carlo method respectively. The results show that the uncertainties from the experimental dispersion calibration (mostly less than 1%) are mostly covered by the range from the models (less than 10%). The sampling efficiency of 5 nm particles displays larger uncertainty than

bigger particles, especially for the measured data. This confirms that the detection limit of the Condensation particle counter and the atomizer is close to 5 nm. Compared with particle collection with a 1.2 μm filter at 0.6 L/min flowrate, the uncertainties from models reduce (the minimum reduces from 5% to 1%) when using a large pore size (2 μm) filter or sampling at a low flowrate (0.4 L/min) because the Cunningham correction factor is removed in the Stokes number calculation. The contribution of parameters involved in the models to the uncertainties of theoretical sampling efficiency was quantified by Sobol variance-based sensitivity analysis. The results demonstrate that for small particles, the filter pore size and the Cunningham correction factor add significant uncertainties to the model uncertainties; for large particles, the flowrate is also a primary parameter. The pore size and flowrate require control to enhance the precision of sampling efficiency. The choice of models and parameter values is essential for simulating the sampling efficiency under different conditions. These results give opportunities to decrease the sampling efficiency uncertainty by controlling the parameter range and provide a basis for the MPS sampling system applications, such as the nanomaterial exposure risk assessment.

References

[1] T. Avanesian, S. Dai, M. J. Kale, G. W. Graham, X. Pan, P. Christopher, Quantitative and atomic-scale view of CO-induced Pt nanoparticle surface reconstruction at saturation coverage via DFT calculations coupled with in situ TEM and IR, J. Am. Chem. Soc., 139 (2017) 4551-4558.

[2] L. Liu, D. N. Zakharov, R. Arenal, P. Concepcion, E. A. Stach, A. Corma, Evolution and stabilization of subnanometric metal species in confined space by in situ TEM, Nat. Commun., 9 (2018) 1-10.

[3] F. Loosli, J. Wang, S. Rothenberg, M. Bizimis, C. Winkler, O. Borovinskaya, L. Flamigni, M. Baalousha, Sewage spills are a major source of titanium dioxide engineered (nano)-particle release into the environment, Environ. Sci. Nano, 6 (2019) 763-777.

[4] M. L. Oliveira, K. Da Boit, I. L. Schneider, E. C. Teixeira, T. J. C. Borrero, L. F. Silva, Study of coal cleaning rejects by FIB and sample preparation for HR-TEM: mineral surface chemistry and nanoparticle-aggregation control for health studies, J. Clean. Prod., 188 (2018) 662-669.

[5] M. G. Ammendolia, F. Iosi, F. Maranghi, R. Tassinari, F. Cubadda, F. Aureli, A. Raggi, F. Superti, A. Mantovani, B. De Berardis, Short-term oral exposure to low doses of nano-sized TiO2 and potential modulatory effects on intestinal cells, Food Chem. Toxicol., 102 (2017) 63-75.

[6] I. Park, H. Kim, S. Lee, Characteristics of tire wear particles generated in a laboratory simulation of tire/road contact conditions, J. Aerosol Sci., 124 (2018) 30-40.

[7] C. Tsai, A. Castano, J. Khattak, M. Ellenbecker, Nano particle Collection by Various Sampling Techniques for Worker Exposure Assessment, Int J Occup Environ Hyg: IJOEH-105, 10 (2018).

[8] M. Fierz, D. Meier, P. Steigmeier, H. Burtscher, Miniature nanoparticle sensors for exposure measurement and TEM sampling, J. Phys. Conf. Ser., (2015) 012034.

[9] A. Miller, G. Frey, G. King, C. Sunderman, A handheld electrostatic precipitator for sampling airborne

particles and nanoparticles, Aerosol Sci. Technol., 44 (2010) 417-427.

[10] J. Lyyränen, U. Backman, U. Tapper, A. Auvinen, J. Jokiniemi, A size selective nanoparticle collection device based on diffusion and thermophoresis, J. Phys. Conf. Ser., (2009) 012011.

[11] B. R'mili, C. Dutouquet, J. Sirven, O. Aguerre-Chariol, E. Frejafon, Analysis of particle release using LIBS (laser-induced breakdown spectroscopy) and TEM (transmission electron microscopy) samplers when handling CNT (carbon nanotube) powders, J. Nanopart. Res., 13 (2011) 563-577.

[12] D. Leith, D. Miller-Lionberg, G. Casuccio, T. Lersch, H. Lentz, A. Marchese, J. Volckens, Development of a transfer function for a personal, thermophoretic nanoparticle sampler, Aerosol Sci. Technol., 48 (2014) 81-89.

[13] C. S. J. Tsai, D. Theisen, A sampler designed for nanoparticles and respirable particles with direct analysis feature, J. Nanopart. Res., 20 (2018) 209.

[14] S. J. C. Tsai, E. Ada, J. A. Isaacs, M. J. Ellenbecker, Airborne nanoparticle exposures associated with the manual handling of nanoalumina and nanosilver in fume hoods, J. Nanopart. Res., 11 (2009) 147-161.

[15] B. R'mili, O. L. Le Bihan, C. Dutouquet, O. Aguerre-Charriol, E. Frejafon, Particle sampling by TEM grid filtration, Aerosol Sci. Technol., 47 (2013) 767-775.

[16] M. Xiang, M. Morgeneyer, O. Aguerre-Chariol, F. Philippe, C. Bressot, Airborne nanoparticle collection efficiency of a TEM grid-equipped sampling system. Aerosol Sci. Technol., (2021) 1-19.

[17] I. Ogura, N. Hashimoto, M. Kotake, H. Sakurai, A. Kishimoto, K. Honda, Aerosol particle collection efficiency of holey carbon film-coated TEM grids, Aerosol Sci. Technol., 48 (2014) 758-767.

[18] S. Bourrous, Q. Ribeyre, L. Lintis, J. Yon, S. Bau, D. Thomas, C. Vallières, F. X. Ouf, A semi-automatic analysis tool for the determination of primary particle size, overlap coefficient and specific surface area of nanoparticles aggregates, J. Aerosol Sci., 126 (2018) 122-132.

[19] O. Le Bihan, C. Bressot, M. Dalle, L. Meunier, O. Aguerre-Chariol, Aerosol nanostructure study with porous grids-A review, J. Phys. Conf. Ser., (2016) 16.

[20] C. Bressot, N. Manier, C. Pagnoux, O. Aguerre-Chariol, M. Morgeneyer, Environmental release of engineered nanomaterials from commercial tiles under standardized abrasion conditions, J. Hazard. Mater., 322 (2017) 276-283.

[21] C. Bressot, N. Shandilya, T. Jayabalan, G. Fayet, M. Voetz, L. Meunier, O. Le Bihan, O. Aguerre-Chariol, M. Morgeneyer, Exposure assessment of Nanomaterials at production sites by a Short Time Sampling (STS) approach: Strategy and first results of measurement campaigns, Process Saf Environ Prot., 116 (2018) 324-332.

[22] N. Shandilya, O. Le Bihan, C. Bressot, M. Morgeneyer, Emission of titanium dioxide nanoparticles from building materials to the environment by wear and weather, Environ. Sci. Technol., 49 (2015) 2163-2170.

[23] M. Morgeneyer, O. Aguerre-Chariol, C. Bressot, STEM imaging to characterize nanoparticle emissions and help to design nanosafer paints, Chem Eng Res Des., 136 (2018) 663-674.

[24] P. Zhao, Y. Zhang, The Overview of Methods of Nanoparticle Exposure Assessment, Methods Mol. Biol., 1894 (2019) 353-367.

[25] C. Soize, Random matrix theory for modeling uncertainties in computational mechanics, Comput. Methods Appl. Mech. Eng., 194 (2005) 1333-1366.

[26] N. Metropolis, S. Ulam, The monte carlo method, J. Am. Stat. Assoc., 44 (1949) 335-341.

[27] C. P. Robert, G. Casella, G. Casella, Introducing monte carlo methods with r, Springer, 2010.

[28] EC, Impact assessment guidelines, Technical Report, 2009.

[29] EPA, Guidance on the development, evaluation, and application of environmental models, in: C.f.R.E. Modeling, Technical report, Office of the Science Advisor, 2009.

[30] H. Chen, Z. Zhang, Z. Zhang, F. Jiang, R. Du, Enhancement of filtration efficiency by electrical charges on nebulized particles, Particuology, 37 (2018) 81-90.

[31] R. Givehchi, Q. Li, Z. Tan, The effect of electrostatic forces on filtration efficiency of granular filters, Powder Technol., 277 (2015) 135-140.

[32] A. Wiedensohler, An approximation of the bipolar charge distribution for particles in the submicron size range, J. Aerosol Sci., 19 (1988) 387-389.

[33] S. C. Chen, J. Wang, H. Fissan, D. Y. H. Pui, Use of nuclepore filters for ambient and workplace nanoparticle exposure assessment—spherical particles, Atmos. Environ., 77 (2013) 385-393.

[34] C. M. Romo-Kröger, Measurable electrostatic effects in nuclepore filters, Japca, 39 (1989) 1465-1466.

[35] W. C. Hinds, Aerosol technology: Properties, behavior, and measurement of airborne particles, 2nd ed., John Wiley & Sons, New York, 1999.

[36] Workplace exposure-assessment of sampler performance for measurement of airborne particle concentration, Part 2: Laboratory performance test based on determination of sampling efficiency, in: Association Feancaise de Normalisation (AFNOR), 2014.

[37] M. Manton, The impaction of aerosols on a nuclepore filter, Atmos. Environ., 12 (1978) 1669-1675.

[38] M. Manton, Brownian diffusion of aerosols to the face of a nuclepore filter, Atmos. Environ., 13 (1979) 525-531.

[39] K. L. Rubow, Submicron Aerosol Filtration Characteristics of Membrane Filters, in: University of Minnesota, 1981.

[40] K. Spurny, J. P. Lodge, E. R. Frank, D. C. Sheesley, Aerosol filtration by means of Nuclepore filters: structural and filtration properties, Environ. Sci. Technol., 3 (1969) 453-464.

[41] P. Bulejko, Numerical Comparison of Prediction Models for Aerosol Filtration Efficiency Applied on a Hollow-Fiber Membrane Pore Structure, Nanomaterials, 8 (2018) 447.

[42] S. Marre, J. Palmeri, Theoretical study of aerosol filtration by nucleopore filters: the intermediate crossover regime of Brownian diffusion and direct interception, J. Colloid Interface Sci., 237 (2001) 230-238.

[43] M. Xiang, M. Morgeneyer, F. Philippe, M. Manokaran, C. Bressot, Comparative review of efficiency analysis for airborne solid submicrometer particle sampling by nuclepore filters, Chem. Eng. Res. Des., 164 (2020) 338-351.

[44] M. Z. Li, Z. Y. Cai, Z. Sui, Q. Yan, Multi-point forming technology for sheet metal, J. Mater. Process. Technol., 129 (2002) 333-338.

[45] J. Pich, Impaction of aerosol particles in the neighbourhood of a circular hole, Collect. Czech. Chem. Commun., 29 (1964) 2223-2227.

[46] L. Coquelin, L. Le Brusquet, N. Fischer, F. Gensdarmes, C. Motzkus, T. Macé, G. Fleury, Uncertainty propagation using the Monte Carlo method in the measurement of airborne particle size distribution with a scanning mobility particle sizer, Meas. Sci. Technol., 29 (2018) 055801.

[47] Evaluation of measurement data — Guide to the expression of uncertainty in measurement, in: Geneva, 2008.

[48] R. T. Birge, The 1944 values of certain atomic constants with particular reference to the electronic

charge, Am. J. Phys., 13 (1945) 63-73.

[49] A. Maali, S. Colin, B. Bhushan, Slip length measurement of gas flow, Nanotechnology, 27 (2016) 374004.

[50] S. Marre, J. Palmeri, A. Larbot, M. Bertrand, Modeling of submicrometer aerosol penetration through sintered granular membrane filters, J. Colloid Interface Sci., 274 (2004) 167-182.

[51] J. H. Kim, G. W. Mulholland, S. R. Kukuck, D. Y. Pui, Slip correction measurements of certified PSL nanoparticles using a nanometer differential mobility analyzer (Nano-DMA) for Knudsen number from 0.5 to 83, J. Res. Natl. Inst. Stand. Technol., 110 (2005) 31.

[52] Determination of particle size distribution-differential electrical mobility analysis for aerosol particles, in: British Standards Institute, 2009.

[53] M. D. Allen, O. G. Raabe, Slip correction measurements of spherical solid aerosol particles in an improved Millikan apparatus, Aerosol Sci. Technol., 4 (1985) 269-286.

[54] D. Hutchins, M. Harper, R. Felder, Slip correction measurements for solid spherical particles by modulated dynamic light scattering, Aerosol Sci. Technol., 22 (1995) 202-218.

[55] H. Jung, G. W. Mulholland, D. Y. Pui, J. H. Kim, Re-evaluation of the slip correction parameter of certified PSL spheres using a nanometer differential mobility analyzer (NDMA), J. Aerosol Sci., 51 (2012) 24-34.

[56] I. Y. M. Sobol', Sensitivity estimates for nonlinear mathematical models, Mat. Model., 2 (1990) 112–118.

[57] I. Y. M. Sobol', Sensitivity analysis for non-linear mathematical models, Mathematical Modeling & Computational Experiment (Engl. Transl.), 1 (1993) 407–414.

[58] A. Saltelli, M. Ratto, T. Andres, F. Campolongo, J. Cariboni, D. Gatelli, M. Saisana, S. Tarantola,

Global sensitivity analysis: the primer, John Wiley & Sons, 2008.

[59] I. M. Sobol, Global sensitivity indices for nonlinear mathematical models and their Monte Carlo estimates, Math. Comput. Simul., 55 (2001) 271-280.

[60] T. Homma, A. Saltelli, Importance measures in global sensitivity analysis of nonlinear models, Reliab. Eng. Syst. Saf., 52 (1996) 1–17.

[61] M. B. Attoui, de la Mora, J. Fernadez, On the Detection Limit of Hydrophilic Particles by a Water CPC, Presentation, European Aerosol Conference, Ghent, Belgium, August 28 - September 2, 2005.

[62] T. N. Smith, C. R. Phillips, O. T. Melo, Diffusive collection of aerosol particles on Nuclepore membrane filter, Environ. Sci. Technol., 10 (1976) 274-277.

[63] G. Glen, K. Isaacs, Estimating Sobol sensitivity indices using correlations, Environ. Modell. Software, 37 (2012) 157-166.

[64] J. Gentry, K. Spurny, J. Schoermann, Diffusional deposition of ultrafine aerosols on nuclepore filters, Atmos. Environ., 16 (1982) 25-40.